Author/s:
Zhao, P;Kim, BJ;Ren, X;Lee, DG;Bang, GJ;Jeon, JB;Kim, WB;Jung, HS

Title:
Antisolvent with an Ultrawide Processing Window for the One-Step Fabrication of Efficient and Large-Area Perovskite Solar Cells

Date:
2018-12-06

Citation:
Zhao, P., Kim, B. J., Ren, X., Lee, D. G., Bang, G. J., Jeon, J. B., Kim, W. B. & Jung, H. S. (2018). Antisolvent with an Ultrawide Processing Window for the One-Step Fabrication of Efficient and Large-Area Perovskite Solar Cells. ADVANCED MATERIALS, 30 (49), https://doi.org/10.1002/adma.201802763.

Persistent Link:
https://hdl.handle.net/11343/285024

DOI: 10.1002/((please add manuscript number))

**Article type: Communication**



# Antisolvent with an Ultrawide Processing Window for the One Step Fabrication of Efficient and Large Area Perovskite Solar Cells

*Pengjun Zhao[†], Byeong Jo Kim[†], Xiaodong Ren[†], Dong Geon Lee, Gi Joo Bang, Jae Bum Jeon, Won Bin Kim, and Hyun Suk Jung[*]*

Dr. P. J. Zhao[†], Dr. B. J. Kim[†], Dr. X. D. Ren[†], Mr. D. G. Lee, Mr. G. H. Bang, Mr. J. B. Jeon, Mr. W. B. Kim, and Prof. H. S. Jung

School of Advanced Materials Science & Engineering

Sungkyunkwan University, Suwon, 440-746, Korea

Corresponding author: Hyun Suk Jung

E-mail: hsjung1@skku.edu

[†] P.J.Z., B.J.K. and X. R contributed equally to this work.

Keywords: perovskite solar cells, anisole, antisolvent, hydrogen bonding, process window

Perovskite absorber materials based photovoltaic technologies have led this optoelectronic field into a brand-new horizon. Yet the present antisolvents used in the one-step spin-coating method always encounter problems with the very narrow process window. In this report, we introduced anisole into the one-step spin-coating method and developed the technology to fabricate perovskite thin films with ultra-wide processing window with a dimethylformamide (DMF): dimethyl sulfoxide (DMSO) ratio varying from 6:4 to 9:1 in the precursor solution, anisole dripping time ranging from 5 to 25 s, and an antisolvent volume varying from 0.1 to 0.9 ml. We have successfully fabricated perovskite thin films as large as 100 $cm^2$ using this method. We obtained a maximum photoelectric conversion efficiency of 19.76% for a small area (0.14 $cm^2$) and 17.39% for a large area (1.08 $cm^2$) perovskite solar cell devices. We also found that there are intermolecular hydrogen-bonding forces between anisole and DMF/ DMSO that plays critical roles in the wide process window. These results provide a deeper understanding of the crystallizing procedure of perovskite during the one-step spin-coating process.

Inorganic-organic hybrid perovskite solar cells (PSC) have been considered as the most promising next generation thin-film photovoltaic devices due to their dramatic development during the past five years. Certified photoelectric conversion efficiency (PCE) for small area PSC (0.095 $cm^2$) as high as 22.7 %,[1] 19.7 % for 1.0 $cm^2$, and 12.1 % for large area of 36.1 $cm^2$[2] have been achieved. The foremost component in a PSC device is the perovskite structured organic metal halide thin film. Up to date, several approach have been applied to fabricate the perovskite thin film on electron transport layers (ETL) or hole transport layers (HTL) including vacuum vapor deposition[3] and non-vacuum one-step[4]/two-step solution deposition[5] methods.

Among above methods, the most common strategy is the one-step spin-coating deposition assisted by an antisolvent, which is an easy and efficient approach to obtain dense and highly crystalline perovskite thin film. Three organic solvents: chlorobenzene (CB),[4b] methylbenzene (toluene)[4a] and diethyl ether (ether)[4c] are the favourite antisolvents for this method. Efficient PSCs with PCE over 20% have been frequently obtained by using these antisolvents,[6] through the one-step spin-coating method.

Three dominant parameters related to the one-step spin-coating process are: (1) the ratio between DMF/DMSO in the perovskite precursor solution, (2) the antisolvent dripping time during the spin procedure and (3) the antisolvent volume used for each coating process as depicted in **Figure 1a**. However, the current antisolvents mentioned above usually have very narrow and various operating windows. For instance, from the point of view of DMF/DMSO ratio, the proper value for CB is 4:1,[7] toluene is 7:3,[4a] while ether is 9:1.[4c] Meanwhile, the dripped antisolvent volume for each antisolvent is also different from case to case: 0.1 ml for CB, 0.5-1.0 ml for toluene and 0.5 ml for

ether.[4a, 4c, 6a, 7] This actuality means that only skillful experimenters can handle the spin-coating tricks and thus fabricate PCEs with high efficiency, which limits the development of the PSCs.

Herein, we would like to introduce anisole as an antisolvent, with ultra-wide processing window for the one-step fabrication of efficient and large area PSCs. Using the anisole as antisolvent, there is no need to make any significant effort to obtain optimized conditions for the fabrication of high quaility perovskite films (**Figure 1b**). By dripping anisole on the spinning perovskite precursor film, it is possible to make dense and cristalline perovskite films as shown in **Figures 1c and d**. The thickness of the perovskite capping layer is about 450 nm, which is comparable with the perovskite thin films using the other antisolvents with optimized condition.[7-8]

Table 1. The average photovoltaic parameters of PSCs form Anisole antisolvent

| **Parameters** | **$J_{sc}$(mA cm$^{-2}$)** | **$V_{oc}$ (V)** | **FF** | **PCE (%)** |
|---|---|---|---|---|
| **Anisole Dripping Time** | | | | |
| **5s** | 21.54 ±0.13 | 1.118 ±0.0098 | 0.737 ±0.0122 | 17.77 ±0.46 |
| **10s** | 21.45 ±0.23 | 1.117 ±0.0094 | 0.738 ±0.0116 | 17.70 ±0.56 |
| **15s** | 21.56 ±0.16 | 1.123 ±0.0112 | 0.748 ±0.0093 | 18.10 ±0.50 |
| **20s** | 21.67 ±0.13 | 1.129 ±0.0098 | 0.753 ±0.0121 | 18.42 ±0.52 |
| **25s** | 21.35 ±0.23 | 1.138 ±0.0050 | 0.757 ±0.0040 | 18.39 ±0.24 |
| **Anisole Dripping Volume** | | | | |

| | | | | |
|---|---|---|---|---|
| **0.1 mL** | 21.00 ±0.28 | 1.137 ±0.0097 | 0.747 ±0.0077 | 17.83 ±0.46 |
| **0.3 mL** | 21.37 ±0.25 | 1.137 ±0.0077 | 0.755 ±0.0064 | 18.35 ±0.49 |
| **0.5 mL** | 21.35 ±0.26 | 1.138 ±0.0056 | 0.757 ±0.0045 | 18.39 ±0.27 |
| **0.7 mL** | 21.26 ±0.38 | 1.140 ±0.0079 | 0.755 ±0.0082 | 18.31 ±0.46 |
| **0.9 mL** | 21.47 ±0.74 | 1.148 ±0.0082 | 0.753 ±0.0158 | 18.54 ±0.84 |
| **DMF:DMSO ratio (V:V)** | | | | |
| **6:4** | 21.88 ±0.26 | 1.152 ±0.0072 | 0.746 ±0.0125 | 18.80 ±0.36 |
| **7:3** | 21.88 ±0.24 | 1.150 ±0.0057 | 0.744 ±0.0153 | 18.72 ±0.41 |
| **8:2** | 21.78 ±0.20 | 1.146 ±0.0056 | 0.736 ±0.0168 | 18.38 ±0.36 |
| **9:1** | 21.69 ±0.21 | 1.132 ±0.0131 | 0.722 ±0.0264 | 17.74 ±0.77 |

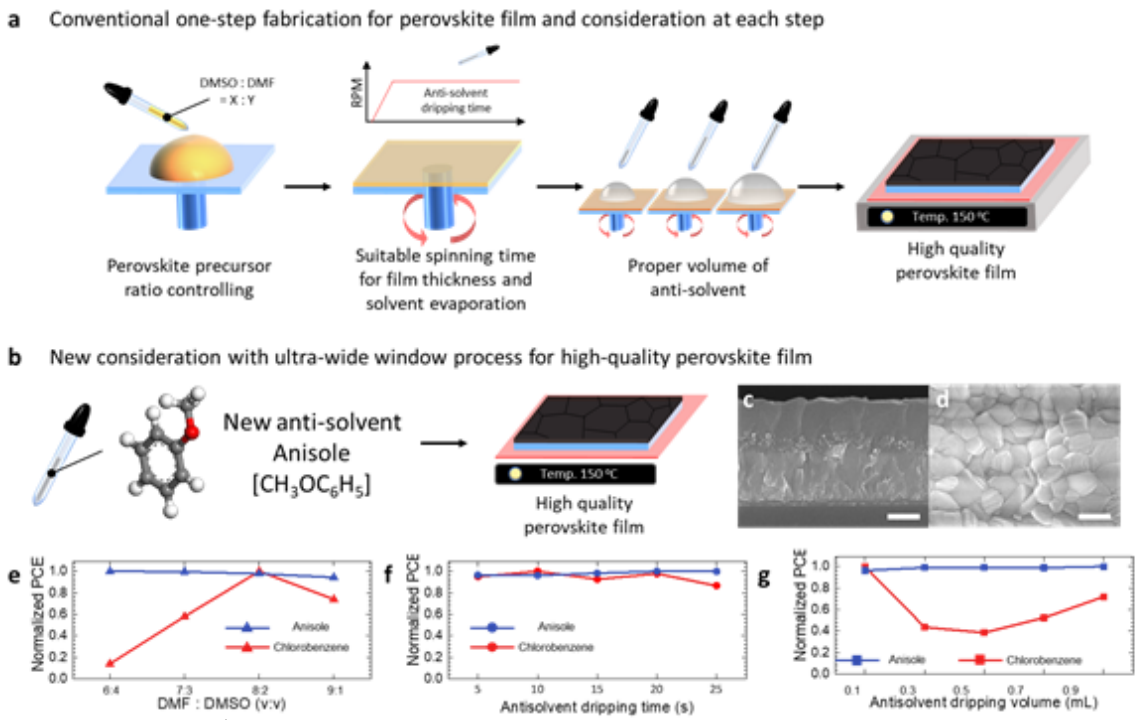


Figure 1. Schematic diagrams to display the procedure of one-step spin-coating perovskite thin films by using (a) conventional antisolvents and (b) Anisole; the representative surface (c) and cross-sectional (d) SEM images of the perovskite thin film fabricated by Anisole (Scale bar = 200 nm); comparisons of the normalized PCE between PSCs fabricated from thin films by Anisole and Chlorobenzene using various process parameters: (d) DMF: DMSO ratio from 6:4 to 9:1, (e) Antisolvent dripping time from 5 to 25 s and (f) Antisolvent dripping volume from 0.1 to 0.9 ml.

Also, the PCEs of PSCs fabricated using anisole are not sensitive to the precursor solution composition and antisolvent dripping parameters. We prepared perovskite thin films using the one-step spin coating method using four kinds of antisolvent: anisole, CB, toluene and ether as antisolvents under different process conditions. There are 14 kinds of various antisolvent treatment

conditions applied in this report, divided into three groups: (1) DMF/DMSO ratios: 6:4, 7:3, 8:2, 9:1; (2) antivolent dripping times: 5 s, 10 s, 15 s, 20 s, and 25 s after reaching the maximum spin speed (the total coating time is set as 30s); (3) antisolvent dripping volume: 0.1 ml, 0.3 ml, 0.5 ml, 0.7 ml and 0.9 ml. Futher we fabricated the $TiO_2$/perovskite/Spiro-OMeTAD/Ag structured PSCs based on the as-prepared perovskite thin films above. The obtained normalized PCEs using anisole and CB antisolvents are displayed in **Figure 1e-g**. In addition, those data from toluene and ether are presented in **Figure S3** and **S4**, respectively. It can be observed from **Figure S1a-c** and **Table 1** that the average PCEs fabricated with all the 14 processing parameters exhibit high and unvarying efficiencies (over 18%), which means that the anisole antisolvent brings ultra-wide processing window to fabrication of perovskite films. In contrast, other antisolvents have different individual processing windows. For example, for CB, showed in **Figure 1e-g** and **Table S1**, the optimized DMF/DMSO ratio is 8:2 (4:1) and the CB volume is 0.1 ml, while the average PCEs are not so sensitive to the dripping time. We also summarized the processing windows of toluene and ether in **Figure S3a-c and S4a-c**. In case of toluene, optimized PCE shows at DMF/DMSO ratio of 7:3, dripping time of 10-15 s, and dripping volume of 0.5-0.7 ml. In case of ether, optimized PCE shows at DMF/DMSO=9:1, dripping time of 10-20 s, and driping volume of 0.5 ml. These results are in accordance with the previous reports.[4a, 4c] The average photovoltaic parameters of PSCs by toluene and ether are listed in the **Table S2** and **S3**, respectively.

The impacts of the processing parameters are mainly embodied in the morphology of the perovskite thin films.[4b, 4c] in the **Figure S1d**, anisole treated prerovskite films present similar uniform covered, mirror-like and black perovskite thin films on 2×2 $cm^2$ glass/fluorine-doped tin oxide (FTO)/$TiO_2$ substrates under all processing conditions. Also, In **Figure S1e**, the film thicknesses from different

processing parameters are identical, and all of the 12 samples exhibited an approximate equivalent dense film with a thickness of 430-460 nm. However, the macroscopic features of the perovskite thin films using other antisolvents are various from case to case (**Figure S2, S3d and S4d)**. Thin films obtained using parameters outside of the operating window (dashed circles in **Figure S2, S3d and S4d**) usually displays frosted or inhomogeneous surface, which induces poor photovoltaic performances of the perovskite solar cells under the corresponding processing parameters.

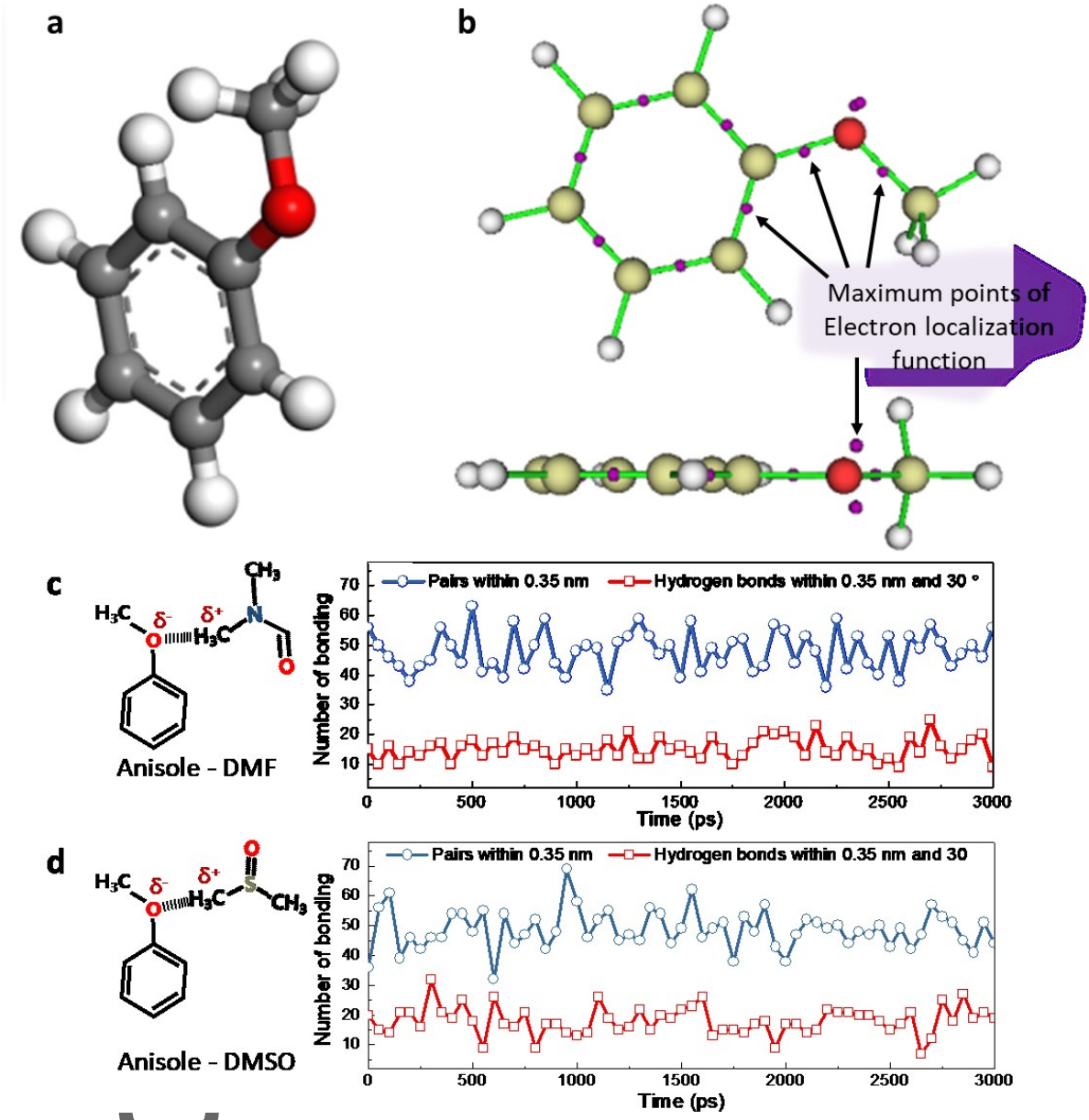


Figure 2. (a) Molecular structure of Anisole; (b) Maximum points in Anisole molecular based on the electron localization function calculation; calculated hydrogen bonding quantity between (c) Anisole-DMF and (d) Anisole-DMSO.

We believe that the reason that the anisole based perovskite thin films have an ultra-wide processing window is due to the hydrogen-bonding induced intermolecular interaction between anisole and DMF/DMSO. From the molecular structure of anisole **Figure 2a**, the –O– group in the molecular center contains, two asymmetric groups, $–C_6H_5$ and $–CH_3$, aside the O atom. Electron Localization Function (ELF) Topology Analysis in **Figure 2b** shows the ELF maximum points (purple dots) in the anisole molecule. Besides the covalent bond between the two atoms, the ELF maximum point also appears in the lone electron pairs of the –O– atom, which is an essential requirements for the formation of hydrogen bonds.[9] The anisole molecule can provide hydrogen-bonding acceptor –O, which is capable of forming hydrogen bonds C-H…O with the C-H donors in the DMSO and DMF molecules.

We calculated the hydrogen-bonding quality in the anisole-DMF and anisole-DMSO systems using the molecular dynamics simulation software from Gromacs. In **Figure 2c and d**, we set two different definitions of hydrogen-bonding: (1) Red line with square box: C-H···O, the distance between C and O is less than 0.35 nm, and the angle between C-H···O is less than 30°; (2) Blue line with circle: C-H···O, the distance between C and O is less than 0.35 nm, but there are no limitation about the angle between C-H···O. the red line with square can be noted from the images that hydrogen-bonding exists both in the anisole-DMF and anisole-DMSO systems. The number of bonding within 35 nm in anisole-DMF and anisole-DMSO are similar to 48.15 and 48.66 on average, however considering the angle (within 30°), the average values are 15.16 in anisole-DMF and 18.12 in anisole-DMSO. So, the number of hydrogen-bonds in anisole-DMSO is a little highher than that of in the anisole-DMF system.

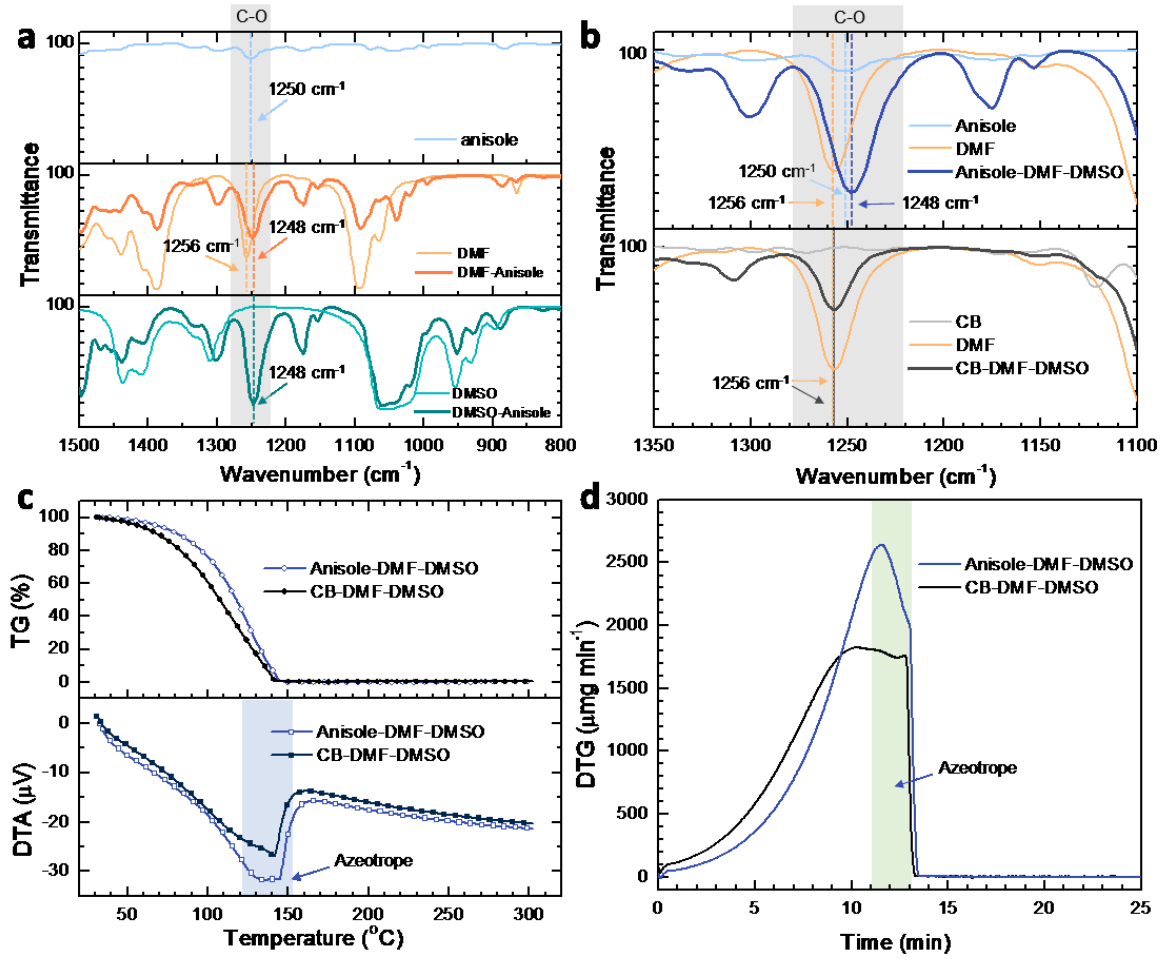


Figure 3. FTIR spectrum of (a) Anisole-DMF-DMSO and (b) CB-DMF-DMSO solvents; (c) TG (top) and TGA (bottom) profiles of Anisole-DMF-DMSO and CB-DMF-DMSO solvents; (d) the corresponding DTG profile to show the Azeotrope in Anisole-DMF-DMSO solvents.

To verify these calculation results, we carried out the Fourier Transform Infrared Spectroscopy (FTIR) analysis by utilizing antisolvents, DMF, DMSO and mixed solvents systems. The FTIR test results of the anisole, anisole-DMF, and anisole-DMSO as well as that of the single DMF and DMSO

solvent are displayed in **Figure 3a**. Generally, if there are intermolecular forces (such as hydrogen-bonding) between two solvents, the corresponding vibration would shift and the intensity would also increases.[10] From **Figure 3a**, it can be noticed that the C-O vibration peak (1250 $cm^{-1}$)[11] is weak for the original anisole (black profile), while this vibration peak shifts for both anisole-DMSO and anisole-DMF to lower wavenumbers and higher intensities. In **Figure 3b**, C-O vibration peak of anisole-DMF-DMSO shows same behavior. On the other hand, FTIR result of CB did not shows specific interaction with the DMF/DMSO solution in the finger printer region (**Figure 3b**), and it was similiar in the other two antisolvent (Toluene and ether, **Figure S5**). In addition, the C-O vibration peak in anisole-DMSO is more intense than that in anisole-DMF, implying that the interaction force between anisole and DMSO is stronger than the one between anisole and DMF. This inference matched the calculation results. Thus, we have demonstrated the existence of the intermolecular hydrogen bonds between anisole and DMF/DMSO, which are responsible for the wide process window of anisole.

Typically, there are four stages during the fabrication process of the perovskite thin film by one-step spin-coating method: i) the first 2-3 seconds, involve removing of the excess precursor perovskite solution by centrifugation; ii) washing out of the residue DMF solvent after dripping the antisolvent,; iii) evaporation of the antisolvent and intermediate phase ($PbI_2$-DMSO-MAI) forms;[4b] and iv) baking the perovskite thin film to remove the DMSO from intermediate phase, and the crystallization of the perovskite grains.

Anisole has a relatively high boiling point (BP) of 153.8 °C, and high viscosity of 1.52 MPa·s, which is about 7 times higher than ether and 3 times higher than CB and toluene (**Table S4**). These features of anisole allow it to form a thin layer with DMF/DMSO after dripping on the perovskite precursor

substrate surface, which protects the thin film from drying after dripping of anisole during stage iii. Meanwhile, since that the BP of anisole is close to that of DMF and DMSO, we deduce that the anisole-DMF-DMSO mixed solvents can form azeotrope. To attest this conclusion, we have proceeded with a Thermogravimetry (TG)-Differential Thermal Analysis (DTA) test by using the mixture of anisole/DMF/DMSO, CB/DMF/DMSO, ether/DMF/DMSO and toluene /DMF/DMSO. It is obvious from **Figure 3c** that the anisole/DMF/DMSO exhibits a distinctive profile for the DTA curve: a platform line at the temperature of 130-150℃, while the other mixture solvents do not show this phenomenon as depicted in **Figure 3c and S6a**. This persistent and constant endothermic line implies that the solvent in the tested crucible was boiling. Furthermore, we drew the derivative thermogravimetry (DTG) profiles for each hybrid solution. As seen in **Figure 3d**, the DTG profile of the anisole-DMF-DMSO solution is made up of two regions: an exponential area from 0 to 11 min and a linearity region from 11 to 13 min. The first region can be assigned to the heterogeneous evaporation of the three solvents and the latter to the boiling of the azeotropic solution. The evaporation rate during liquid heating follows the equation (1):

$$u = \left(\frac{p}{\rho}\right) \times \left[\left(\frac{\mu}{2\pi RT}\right)\right]^{0.5} \quad (1)$$

where $u$ is the evaporation rate, $p$ is the saturated vapor pressure ($lgp = -\frac{52.23B}{T+C}$, $B$ *and* $C$ *is*constant), $\rho$ is the density of the solvent; $\mu$ is the molar mass of the solvent, $R$ is a constant, 8.314 J·mol$^{-1}$·K$^{-1}$ and $T$ is the Kelvin temperature. [12]

Before boiling, $T$, and $\mu$ is variable and the evaporation rate ($u$) follows an exponential function, while the solvent achieves an azeotropic point, the $T$ and $\mu$ would be constant, therefore the evaporation rate becomes a linear function. Because of this, the residual anisole-DMF-DMSO is

evaporated from the substrate surface simultaneously during stage iv as mentioned above. This characteristic of the anisole-DMF-DMSO solution does not appear in the conventional antisolvent (**Figure 3d and S6**), this will allow the forming of a flat and dense perovskite thin film.

To investigate effect of anisole, which has strong interaction with DMSO-DMF, on the coated film during spin-coating, FTIR and x-ray diffraction (XRD) analyzes were performed after anisole treatment (after 0.1 ml antisolvent dripping at 10 sec and 0.8 ml antisolvent dripping at 20 sec / befere annealing). As depicted in Figure S7, after the anisole treatment, the cubic phase of the mixed perovskite as well as the intermediate phase were identified. These are different results by the other antisolvents, removing excess DMF solvent and not forming excessive perovskite phase before further heat treatment[13]. In general, relatively low amounts of perovskite phase were detected after antisolvent treatment, but not in the main phase as shown in the **Figure S7**. This phenomenon interpreted that a large amount of perovskite crystals formed due to extracted dmso from intermediate phase by strong interaction of anisole-dmso-dmf. In other words, it is believed that the anisole affects not only the formation of the intermediate phase but also the nucleation occurs, and the nuclei acts as seed in the grow mechanism of the perovskite film during the heat treatment[14]. An additional thing that can be found in the XRD data, in Figure S7a, $PbI_2$ peak was not detected. Usually, $PbI_2$ is detected on the due to the unwanted evaporation of the solvent after antisolvent treatment/before heat treatment condition[13b, 13c, 15]. However, when anisole was used, $PbI_2$ peak was not detected, indicating that anisole effectively protected the drying of coated film and did not excess wash out of DMSO solvent.

From the above discussion, we have revealed the imminent causes for the ultra-wide process window of the Anisole: (1) the intermolecular forces between anisole and DMF/DMSO allow the

anisole to wash out the redundant DMSO which didn't form an intermediate phase with $PbI_2$; (2) the anisole-DMF-DMSO complex adhered on the substrate surface and is difficult to volatilize during the spin-coating due to the formation of the azeotrope, which can protect the mixed phase of intermediate and nuclei of perovskite layer from (a) the drying and irregular premature perovskite film growth and (b) the uniform high-quality perovskite thin film formation by cybic phase perovskite nuclei regularly formed by annealing process.

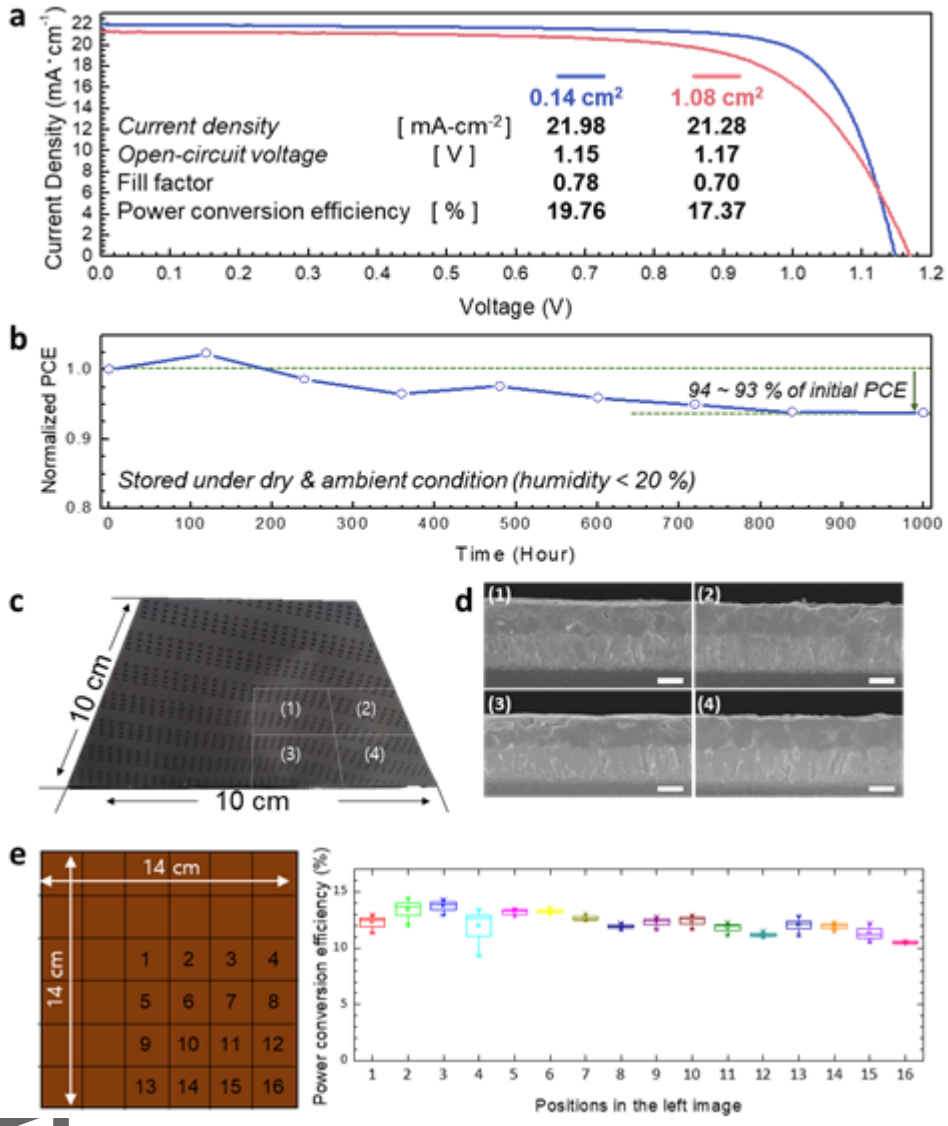

Figure 4. (a) J-V curves of the PSCs devices with 0.14 and 1.08 $cm^2$ fabricated by Anisole as antisolvent; (b) the stability test of the fabricated PSC stored in dry air; (c) The as-prepared perovskite thin film with a size of 100$cm^2$; (d) the cross-sectional SEM images of the perovskite thin films obtained from different section of the thin film in (c) (the scale bar is 200 nm); (e) PCE statistics of the PSCs fabricated form different part of a 196 $cm^2$ perovskite thin film.

To demonstrate the high photovoltaic performance of the anisole based perovskite films, PSCs were fabricated. **Figure 4a** shows the photocurrent density-voltage (*J-V*) curve of PSCs with 0.14 $cm^2$ and 1.08 $cm^2$ of active area. The maximum cell yields a PCE of 19.76%, with a short circuit current density $J_{sc}$= 21.98 mA $cm^{-2}$, open circuit open-voltage $V_{oc}$= 1.15, and fill factor FF= 0.783 at 0.14 $cm^2$. Also, large active area (1.08 $cm^2$) PSCs shows excellent perforamce, obtaning PCE of 17.39 % (redish line in **Figure 4a**, with the following photovoltaic parameters: $J_{sc}$= 21.28 mA $cm^{-2}$, $V_{oc}$= 1.17, fill factor FF= 0.70). We also demonstrate large active area (1.05 $cm^2$) by using CB antisolvent-based PSCs (**Figure S9**).

An inconspicuous hysteresis loop (the PCE difference according to the voltage scan direction is 1% or less) was observed between the forward and reverse direction of the J-V scan (**Figure S8**). In order to evaluate the operation reliability of the device, we performed steady-state photocurrent at maximum power voltage of J-V curve. As seen in **Figure S10b**, the efficiency was stabilized at 17.01% (within 1% of the efficiency measured by the J-V curve in **Figure S10a**). In addition, then fabricated PSC was stored at room terperature in the air (humidity ≤ 20%), and their residual normalized efficiency was 93.7% after 1000 hours (**Figure 4b**).

More importantly than the process window, we also found that the anisole antisolvent treatment is easy to fabricate highly uniform large-scale perovskite thin films. Without modifying any of the spin-coating parameters (spin-coating speed 5000 rpm for 30s and anisole volume was 0.5 ml), we have successfully prepared high quality perovskite thin films with size of 4, 25, 49, 100 and 196 $cm^2$, respectively, and the as-prepared perovskite thin films are presented in **Figure 4c** and **S11**. To verify the uniformity of perovskite films, the thickness and morphorlogy of perovskite film coated on the glass/FTO substrate of over 100 $cm^2$ size. As shown in **Figure 4d**, the cross-sectional thickness of the four parts of the coated perovskite film, approximately the distance from the center of substrate were (1), (2), (3), and (4) shown in **Figure 4c**, was uniform, and the top planar view of the film has similiar shape (**Figure S11**). Also, we fabricated mini-module size planar type PSCs (196 $cm^2$, ETL-free structure which has Glass/FTO/Perovskite/Spiro-MeOTAD/Au) using fully solution processes with anisole antisolvent treatment and divided it into 1 $inch^2$ size (4 electrodes in each small cell, active area : 0.14 $cm^2$) to evaluate PSCs performance. The detailed manufacturing process of 36 small devices using 196 $cm^2$ substrate can be found in the **Figure S12**. **Figure 4d** shows positions and PCE values of the small cells. The average efficiency of 16 devices (64 electrodes) is 12.25 % (strandard deviation : 0.84), the highest efficiency of the center position of the substrate is 14.29 %, and the lowest efficiency at the edge position is 10.35 %. The important point is that the average $J_{sc}$ (20.07 mA/$cm^2$, strandard deviation : 0.42) in entire devices show decent values compared to campion device. However, lower average $V_{oc}$ (1.03 V, standard deviation : 0.01) and lower FF (0.59, srandard deviation : 0.03) has a significant influence on the efficiency variation. As a result, it can be explained that the low efficiency and their distribution of the large area device are due to the low shunt resistance by uniformity HTL (Spiro-MeOTAD) through spin coating and ETL-free device structure.

Therefore, if the perovskite thin film by using anisole is coated into optimized ETL and HTL, a high-efficiency large-area device can be easiliy fabricated.

In summary, a one-step antisolvent assistant spin-coating method for the ultra-wide process window to fabricate the perovskite thin films has been developed, by applying anisole as the antisolvent. The application of these films in n-i-p structured perovskite solar cells led to a maximum PCE of 19.76% for a small active area (0.14 $cm^2$) , 17.39% for a large active area (1.08 $cm^2$), and we demonstrate a large sized conformal perovskite thin film of over 100 $cm^2$ size. We have elaborated that the superiority of anisole is mainly due to its high boiling point, viscosity, as well as the intermolecular interaction between anisole and DMF/DMSO. Also, anisole is thought to be involved in excessive nucleation of perovskite through strong interaction with DMSO. Further investigations on the thin film thickness, precursor recipe and device structure optimization are expected to boost the PSCs' efficiency using anisole-prepared perovskite films. We believe that this thin-film processing technology can be used not only promote the large scale manufacturing of perovskite based photovoltaic devices but also to introduce new deep understanding of the crystallizing procedure of perovskite during the one-step spin-coating process.

*Experimental Section*

*Materials:* All of the chemical reagents are commercial available. $PbI_2$ (99.995%), $PbBr_2$ (99.995%), CsI (99.99%) were purchased from Sigma-Aldrich (U.S.A), and $HC(NH_2)_2I$ (FAI), $CH_3NH_3Br$ (MABr) from Xi'An P-OLED Co. (China).

*Device fabrication:* FTO-coated glass substrates were laser etched by laser, and then rinsed with deionized water, ethanol and acetone. A $TiO_2$ compact layer was then deposited on the substrates by spin-coating method at 4000 r.p.m. for 30s, using a titanium diisopropoxide bis(acetylacetonate) solution (75% in 2-propanol, Sigma-Aldrich) in ethanol (1:19, volume ratio) as precursor and baking for 5 min at 120 °C. The compact $TiO_2$ layer was annealed at 500 °C for 60 min. After that, a $TiCl_4$ water solution (0.04M) was used to treat the $TiO_2$ surface at 70 °C for 20 min and followed by heat treatment at 500 °C for 60 min again. The mesoporous $TiO_2$ layer composed of 30-nm-sized particles was deposited by spin coating at 4,000 r.p.m. for 20 s using a $TiO_2$ paste ((30 NR-D, Greatcell solar, Australia) diluted in ethanol (1:5.5, weight ratio). After drying at 120 °C for 5 min, the $TiO_2$ films were heated to 500 °C, annealed at this temperature for 60 min and cooled to room temperature.

The 1.3 M $[CsPbI_3]_{0.05}[(FAPbI_3)_{0.85}(MAPbBr_3)_{0.15}]_{0.95}$ perovskite precursor solutions were prepared by dissolving corresponding amounts of FAI, MABr, and $PbI_2$ in DMSO/DMF (6:4, 7:3, 8:2 and 1:9 v/v) mixed solvent (5% molar ratio $PbI_2$ excess). The perovskite precursor solution was coated onto the mp-$TiO_2$/bl-$TiO_2$/FTO substrate by using a one-step antisolvent spin-coating method. Briefly, after exposed the substrates under UV-Ozone irradiation for 15 min, the dissolved solution was spin-coated on the substrates at 5000 rpm for 30 s and 0.1-0.9 ml of antisolvent (anisole, CB, toluene, and ether) was slowly dripped (~ 0.2 ml per seconds) on the rotating substrate at 5-25 s after the spin-procedure starting. The semi-transparent film was heated at 150 $^{o}$C for 10 min in order to obtain a dense perovskite film.

After cooling to room temperature, 25 μl HTM was deposited by spin coating at 4,000 r.p.m. for 30 s. The HTM solution consists of 36 mg (2,29,7,79- tetrakis(N,N-di-p-methoxyphenylamine)-9,9-*spiro*bifluorene)- (*spiro*-OMeTAD), 14.4 μl 4-tert-butylpyridine and 8.8 μl of 520 mg $ml^{-1}$ lithium bis(trifluoromethylsulphonyl)imide acetonitrile solution dissolved in 0.5 ml CB. Finally, 80 nm of silver metal was thermally evaporated on top of the device to form the back contact.

*Characterizations*: The current-voltage characteristics of the solar cells were measured using a solar simulator (Newport Oriel Solar 3A Class AAA, 64023A) and a potentiostat (CHI 660D, CH instruments); the measurements were conducted under an illumination of AM 1.5G sun (100 mA $cm^{-2}$), and the potentiostat was calibrated using a standard Si-solar cell (Oriel, VLSI standards) and a light sensor current controller (Newport Oriel digital exposure controller, Model 68945). All devices were measured by masking the active area with a thin mask (0.14 or 1.08 $cm^2$). J-V characteristics for all devices were measured at a voltage scan rate of 0.1 V $s^{-1}$.

SEM images and element contents were obtained from a JSM-7600F hot field emission SEM (JEOL, Japan). FTIR spectra were obtained using a Bruker IFS-66/S, TENSOR27 spectrometer and a scan range of 400-4000 $cm^{-1}$ (wavenumber). The TG/DTA was carried out on a Seiko Exstar 6000 thermal analyzer, and the tested temperature range was from 25 ℃ to 300 ℃ with a heating rate of 10 ℃ per min.

**Supporting Information**

Supporting Information is available from the Wiley Online Library or from the author.

*Acknowledgements*

The authors thank the financial support from the National Research Foundation (NRF) of Korea grant funded by the Korea government (No. 2017R1A2B3010927), Basic Science Research Program through the National Research Foundation of Korea (NRF-2014R1A4A1008474) and Creative Materials Discovery Program (2016M3D1A1027664); Author P. J. Zhao, B. J. Kim and X. D. Ren contributed equally to this article.

References


[1] W. S. Yang, B. W. Park, E. H. Jung, N. J. Jeon, Y. C. Kim, D. U. Lee, S. S. Shin, J. Seo, E. K. Kim, J. H. Noh, S. I. Seok, *Science* **2017**, 356, 1376.

[2] H. Chen, F. Ye, W. T. Tang, J. J. He, M. S. Yin, Y. B. Wang, F. X. Xie, E. B. Bi, X. D. Yang, M. Gratzel, L. Y. Han, *Nature* **2017**, 550, 92.

[3] a) X. Li, D. Bi, C. Yi, J.-D. Décoppet, J. Luo, S. M. Zakeeruddin, A. Hagfeldt, M. Grätzel, *Science* **2016**, DOI: 10.1126/science.aaf8060; b) M. Liu, M. B. Johnston, H. J. Snaith, *Nature* **2013**, 501, 395.

[4] a) N. J. Jeon, J. H. Noh, Y. C. Kim, W. S. Yang, S. Ryu, S. Il Seol, *Nat Mater* **2014**, 13, 897; b) M. D. Xiao, F. Z. Huang, W. C. Huang, Y. Dkhissi, Y. Zhu, J. Etheridge, A. Gray-Weale, U. Bach, Y. B. Cheng, L. Spiccia, *Angew Chem Int Edit* **2014**, 53, 9898; c) N. Ahn, D. Y. Son, I. H. Jang, S. M. Kang, M. Choi, N. G. Park, *Journal of the American Chemical Society* **2015**, 137, 8696.

[5] a) Q. Jiang, L. Zhang, H. Wang, X. Yang, J. Meng, H. Liu, Z. Yin, J. Wu, X. Zhang, J. You, *Nature Energy* **2016**, 2, 16177; b) J. H. Wu, X. Xu, Y. H. Zhao, J. J. Shi, Y. Z. Xu, Y. H. Luo, D. M. Li, H. J. Wu, Q. B. Meng, *ACS applied materials & interfaces* **2017**, 9, 26937; c) J. J. Mo, C. F. Zhang, J. J. Chang, H. F. Yang, H. Xi, D. Z. Chen, Z. H. Lin, G. Lu, J. C. Zhang, Y. Hao, *Journal of Materials Chemistry A* **2017**, 5, 13032; d) M. H. Li, X. Q. Yan, Z. Kang, X. Q. Liao, Y. Li, X. Zheng, P. Lin, J. J. Meng, Y. Zhang, *ACS applied materials & interfaces* **2017**, 9, 7224; e) H. P. Shen, Y. L. Wu, J. Peng, T. Duong, X. Fu, C. Barugkin, T. P. White, K. Weber, K. R. Catchpole, *ACS applied materials & interfaces* **2017**, 9, 5974.

[6] a) N. J. Jeon, J. H. Noh, W. S. Yang, Y. C. Kim, S. Ryu, J. Seo, S. I. Seok, *Nature* **2015**, 517, 476; b) J.-W. Lee, D.-H. Kim, H.-S. Kim, S.-W. Seo, S. M. Cho, N.-G. Park, *Advanced Energy Materials* **2015**, 5, 1501310; c) N. Arora, S. Orlandi, M. I. Dar, S. Aghazada, G. Jacopin, M. Cavazzini, F. Mosconi, P. Gratia, F. De Angelis, G. Pozzi, M. Graetzel, M. K. Nazeeruddin, *ACS Energy Letters* **2016**, 1, 107.

[7] K. T. Cho, S. Paek, G. Grancini, C. Roldán-Carmona, P. Gao, Y. Lee, M. K. Nazeeruddin, *Energy Environ. Sci.* **2017**, 10, 621.

[8] a) D. Q. Bi, W. Tress, M. I. Dar, P. Gao, J. S. Luo, C. Renevier, K. Schenk, A. Abate, F. Giordano, J. P. C. Baena, J. D. Decoppet, S. M. Zakeeruddin, M. K. Nazeeruddin, M. Gratzel, A. Hagfeldt, *Sci Adv* **2016**, 2; b) P. Cui, D. Wei, J. Ji, D. Song, Y. Li, X. Liu, J. Huang, T. Wang, J. You, M. Li, *Solar RRL* **2017**, 1, 1600027.

[9] R. H. Crabtree, *Chem Soc Rev* **2017**, 46, 1720.

[10] a) Y. Furutani, H. Kandori, *Bba-Bioenergetics* **2014**, 1837, 598; b) I. Giannicchi, B. Jouvelet, B. Isare, M. Linares, A. Dalla Cort, L. Bouteiller, *Chemical communications* **2014**, 50, 611; c) Y. Z. Zheng, H. Y. He, Y. Zhou, Z. W. Yu, *J Mol Struct* **2014**, 1069, 140; d) S. A. Qian, W. L. Heng, Y. F. Wei, J. J. Zhang, Y. Gao, *Cryst Growth Des* **2015**, 15, 2920.

[11] a) U. Stafford, K. A. Gray, P. V. Kamat, A. Varma, *Chemical Physics Letters* **1993**, 205, 55; b) O. Seiferth, K. Wolter, B. Dillmann, G. Klivenyi, H. J. Freund, D. Scarano, A. Zecchina, *Surf Sci* **1999**, 421, 176; c) M. M. Paradkar, S. Sakhamuri, J. Irudayaraj, *J Food Sci* **2002**, 67, 2009; d) Y. S. Ch'ng, C. S. Tan, Y. C. Loh, M. Ahmad, M. Z. Asmawi, M. F. Yam, *J Pharmacopunct* **2016**, 19, 145.

[12] a) M. Hong, R. J. Liu, H. X. Yang, W. Guan, J. Tong, J. Z. Yang, *J Chem Thermodyn* **2014**, 70, 214; b) K. Shahbaz, F. S. Mjalli, G. Vakili-Nezhaad, I. M. AlNashef, A. Asadov, M. M. Farid, *J Mol Liq* **2016**, 222, 61.

[13] a) Y. Rong, Z. Tang, Y. Zhao, X. Zhong, S. Venkatesan, H. Graham, M. Patton, Y. Jing, A. M. Guloy, Y. Yao, *Nanoscale* **2015**, 7, 10595; b) K. Sveinbjörnsson, K. Aitola, J. Zhang, M. B. Johansson, X. Zhang, J.-P. Correa-Baena, A. Hagfeldt, G. Boschloo, E. M. J. Johansson, *Journal of Materials Chemistry A* **2016**, 4, 16536; c) N. J. Jeon, J. H. Noh, Y. C. Kim, W. S. Yang, S. Ryu, S. I. Seok, *Nat Mater* **2014**, 13, 897.

[14] a) N.-G. Park, *CrystEngComm* **2016**, 18, 5977; b) Z. Liang, S. Zhang, X. Xu, N. Wang, J. Wang, X. Wang, Z. Bi, G. Xu, N. Yuan, J. Ding, *RSC Advances* **2015**, 5, 60562; c) Y. Zhao, H. Tan, H. Yuan, Z. Yang, J. Z. Fan, J. Kim, O. Voznyy, X. Gong, L. N. Quan, C. S. Tan, J. Hofkens, D. Yu, Q. Zhao, E. H. Sargent, *Nature communications* **2018**, 9, 1607.

[15] N. Ahn, D. Y. Son, I. H. Jang, S. M. Kang, M. Choi, N. G. Park, *J Am Chem Soc* **2015**, 137, 8696.

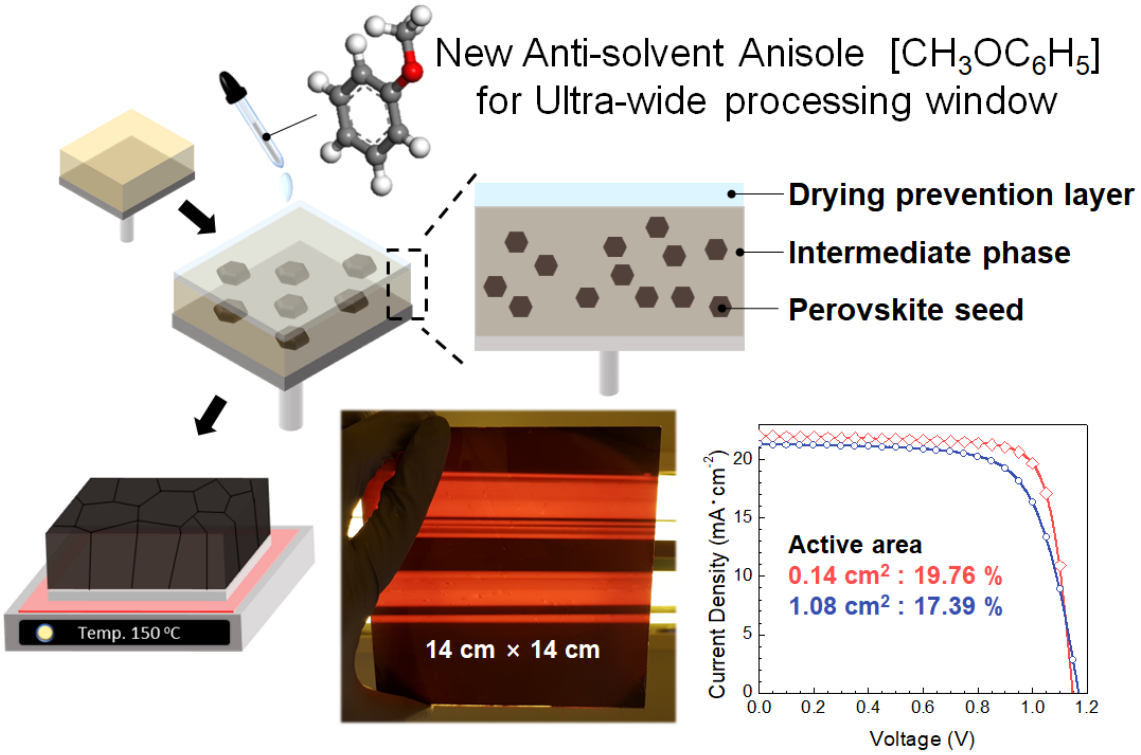


**By applying anisole**, a one-step antisolvent assistant spin-coating method with ultra-wide process window to fabricate the perovskite thin films has been developed. The application of these films in n-i-p structured perovskite solar cells lead to maximum PCE of 19.76% for a small area (0.14 $cm^2$), 17.39% for large area (1.08 $cm^2$), and large sized perovskite thin film of 196 $cm^2$.